# Foam generation and stability: Role of surfactant structure and asphaltene aggregates

*Shirin Alexander[†,*], Andrew R. Barron[†,‡,¶,π*], Nikolai Denkov[ϕ], Paul Grassia[¢], Sajad Kiani[†], Masanobu Sagisaka[¥], Mohammad Javad Shojaei[$], Nima Shokri[#,*]*

[†]Energy Safety Research Institute (ESRI), Swansea University, Bay Campus, Swansea SA1 8EN, UK

[‡]Arizona Institutes of Resilience (AIR), University of Arizona, Tucson, Arizona 85721, USA

[¶]Department of Chemistry and Department of Materials Science and Nanoengineering, Rice University, Houston, Texas 77005, USA

[π]Faculty of Engineering, Universiti Teknologi Brunei, Brunei Darussalam

[ϕ]Department of Chemical and Pharmaceutical Engineering, Faculty of Chemistry and Pharmacy, Sofia University, 1 James Bourchier Avenue, 1164, Sofia, Bulgaria

[¢]Department of Chemical and Process Engineering, University of Strathclyde, Glasgow G1 1XJ, UK

[#]Department of Frontier Materials Chemistry, Graduate School of Science and Technology, Hirosaki University, 3 Bunkyo-cho, Hirosaki, Aomori 036-8561, *Japan*

[$]Department of Earth Science and Engineering, Imperial College London, London, UK

[¥]Hamburg University of Technology, Institute of Geo-Hydroinformatics, Am Schwarzenberg-Campus 3 (E), 21073 Hamburg, Germany

KEYWORDS Foam stability, diffusional coarsening, bubble coalescence, asphaltene aggregate.

**ABSTRACT:** Understanding how the surfactant molecular structure affects foam stability is important in various applications, such as enhanced oil recovery, hydraulic fracturing, and soil remediation. In this study, we conduct a systematic series of experiments in a Hele-Shaw cell to assess and explain the effect of surfactants on the foaminess and foam stability in the absence and presence of oil and asphaltene aggregates. Four surfactants with different molecular weights were studied, incl. three anionic surfactants: sodium 1,5-*bis*[(*1H,1H,2H,2H*-perfluorohexyl)oxy]-1,5-dioxopentane-2-sulfonate (FG4), $C_{18}H_{37}SO_4Na$ (LSES), and sodium dodecyl sulfate (SDS); and one cationic [CTAB, $(C_{16}H_{33}NMe_3)Br$]. The higher electrostatic repulsion between the foam film surfaces for the anionic surfactants (FG4 > LSES > SDS) strongly influences the process of foam generation and stability when compared with cationic (CTAB). Furthermore, the foam experiments performed in the presence of oil revealed maximum long-term stability and minimum bubble coarsening for the partially fluorinated FG4 surfactant. The experiments in the presence of asphaltene-oil mixtures revealed that the latter have detrimental effect on foam stability, except for FG4. The foam experiments clearly show the significance of the subtle interactions between surfactant head-group charge, chain length and branching. The obtained results could be useful in designing appropriate surfactants for foam stabilization in various applications.

## 1. INTRODUCTION

Foam is a dispersed gaseous phase within a continuous of thin liquid films, known as lamellae,[1,2] with applications in soil remediation, the food industry, and enhanced oil recovery projects. The stability of a foam is of great importance for its successful application.[3] Experimental studies demonstrate that foam stability strongly depends on the surfactant structure.[4,5] Surfactants are characterized by a hydrophilic head with the affinity to polar material and a hydrophobic tail with the affinity for non-polar material,[6,7] hence, they can adsorb and reside simultaneously in both hydrophobic and hydrophilic media. At low surfactant concentrations surfactant molecules gradually adsorb on the air-liquid interface and form a monolayer as concentration is increased.[8] Beyond a critical micelle concentration (CMC) an increase in surfactant concentration generates more and more micelles, but does not result in any significant change in surface tension.[9] Micelles are known to play a role in the supply of free surfactant molecules for generating emulsions and bubbles (foam) when oil or air is injected into an aqueous surfactant solution. Some applications using surfactant, such as EOR,[10] are usually carried out under a high salinity condition, which drastically destabilizes and precipitates surfactant micelles by salting-out effect (namely a drastic increase in Krafft temperature or decrease in cloud temperature). Thus, micelles might not even be present in saline systems. On the other hand, a larger number of micelles often cause unwanted side-effects like making demulsification/surfactant-removal processes more energy-consuming and complicated after use. For example, water-oil separation after oil recovery is more difficult at a higher surfactant concentration. Due to the high cost and various risks on the environment and living beings, the dissipation by salting out of surfactant, and the large energy consumption processes after use, an effective and efficient surfactant to generate foams even at CMC (very small amounts of micelles) is worth exploring for

applications. Using low surfactant concentration to generate foam is a potential economic advantage also which has prompted many researchers to limit their foam study to the CMC or even below CMC values with particles in lieu of surfactant used to stabilize foams.[11-13]

Foams that are thermodynamically unstable can be destabilized by four primary mechanisms: (i) film drainage, (ii) coalescence, (iii) gas diffusion and (iv) the effect of hydrocarbons.[14,15] Film drainage, also known as film thinning, happens when the lamellae separating two bubbles undergoes a thinning process,[16] where films coalescence upon become thin enough. Gas diffusion from smaller bubbles with higher pressure to larger bubbles with lower pressure causes the smaller bubbles to eventually disappear.[17] Micelles are known to play role of a gas carrier and to accelerate gas diffusion under high pressure condition such as occurs in an oil or gas reservoir. Employing the surfactant concentration at, or below CMC, foam destabilization processes by gas diffusion will be minimized. Although presence of hydrocarbons does not invariably destabilize a foam,[18] there is a body of literature to suggest that oil often leads to destabilization.[18,19] In the literature, it is not still evident by which mechanism oil destabilized foam; however, it is widely believed oil entering into lamellae and spreading over it and bridging between different lamellae destabilized foam.[19,20]

Recent studies showed the movement of surfactants from the bulk to the water-air interface during foam generation leads to surfactant depletion in the aqueous bulk that significantly influences foam properties.[4,21,22] It is essential to stabilize foam with the lowest surfactant consumption due to the high cost of surfactant. Hence in this work, we only considered surfactants at CMC and not any higher. This research studied foam generation and stability of a novel double short FC chain surfactant (FG4) with a low CMC value alongside a low surface energy anionic hydrocarbon surfactant LSES having a hyper-

methyl-branched chain with low CMC value[23] and a commercial straight-chain cationic hydrocarbon surfactant CTAB with a known high degree of surfactant depletion linked to its low CMC and a commercial straight-chain anionic hydrocarbon surfactant SDS with a high CMC value (less affected by the surfactant depletion). Finding out how different properties of surfactant influence foam stability is relevant for synthesizing new surfactant with a high ability to stabilize foam. To find this out, we performed rheology, and surface tension measurements for the surfactant mentioned above. Although most oils are asphaltenic, there is no study in the literature to investigate the role of asphaltene on foam stability which is the other aim of this study.

## 2. EXPERIMENTAL

**2.1. Materials.** Isostearyl alcohol (≥ 98%) was supplied by Nissan Chemical Industries (Japan). Sodium dodecyl sulfate (SDS), cetyl trimethyl ammonium bromide (CTAB), potassium chloride, sodium chloride, magnesium chloride hexahydrate, calcium chloride, dichloromethane, *p*-toluene sulfonic acid monohydrate, chlorosulfonic acid, sodium hydrogen sulfite, 1,4-dioxane, *1H,1H,2H,2H*-perfluorohexyl, ethanol, and acetone were purchased from Sigma-Aldrich (all ≥99%) and used as received. Ultrapure water (resistivity = 18.2 MΩ cm, Millipore) was used for the synthesis of surfactant and for preparation of the aqueous solutions. The double-chain fluorocarbon (FC) surfactant (FG4, denoted as sodium 1,5-*bis*[(*1H,1H,2H,2H*-perfluorohexyl)oxy]-1,5-dioxopentane-2-sulfonate), and the low surface

energy anionic hydrocarbon (HC) surfactant (LSES, denoted as $C_{18}H_{37}SO_4Na$) were synthesized according to previously published methods.[23-25] Isopar V (a relatively light oil) was supplied from ExxonMobil chemicals. Asphaltene aggregates were extracted and purified (IP143, ASTM D6560) from bitumen (Calgary, Canada).

**2.2. Solution Preparation.** An amount equivalent to the CMC values was added to pure water for each aqueous surfactant solution and stirred on a magnetic stirrer at 30 °C for 30 min. Two 'model' oil phases were prepared and used for the experiments: (a) oil, and (b) asphaltene-oil dispersion. The oil dispersion was prepared by the following procedure: 10 mL of heptane:toluene (70:30 v/v) denoted as heptol was added to 90 mL of oil (Isopar V), and stirred at 30 °C for 2 h on a magnetic stirrer. The asphaltene-oil dispersion was initially prepared by adding 200 mg solid asphaltene aggregates in the heptol (70:30 v/v) and vigorously mixing at 30 °C for 2 h on a magnetic stirrer. The solution was then added to the main oil (asphaltene-heptol:main oil, 1:9 v/v) and mixed for 10 min.

**2.3. Interfacial properties of solutions.** The CMC, surface tensions (σ), and interfacial tension (IFT) of the surfactant solutions were measured by the pendant-drop method using DSA25 (Krüss GmbH, Germany) at 25 °C. The surface tension of water (72 mN. $m^{-1}$) was measured at room temperature. In this study, σ values on both fluid-gas interfaces and fluid-fluid interfaces were analyzed using the Young-Laplace equation via the Krüss-ADVANCE software. The measurements were repeated five times at 25 °C. Figure S1 (Supporting Information) depicted surface tension (σ) and droplet volume of

deionized water solutions of each of the surfactants studied. The solutions' rheological properties were measured in response to the applied forces, over 350 sec on a rheometer (Brookfield DV3T) at 25 °C.

### 2.4. Characterization of Foams

*2.4.1. Foam Generation in Hele-Shaw Cell Experiments.* The Hele-Shaw cell contains two glass plates with dimensions of 32×20 cm and a thickness of 0.6 cm (Figure S2, Supporting Information). The two glass plates were separated using a gasket with 1 mm size which allowed the foam to be injected inside the Hele-Shaw cell. The glass plates were sealed using 10 clamps, on each opposite side of the cell. A port was manufactured at the inlet of the Hele-Shaw cell for placing pressure probes to measure pressure, whilst the outlet was maintained at atmospheric pressure. A lightbox was placed below the cell, illuminating the process to improve image acquisition and analysis. An aqueous foam was generated while simultaneously injecting gas and surfactant through a customized foam generator, which was fitted with a sintered glass disc (P100, Scientific Glass, UK) with a pore size distribution between 40-100 µm. The protocol followed in this research, is reproducible based on previous experiments.[23,24] A mass flow controller (Bronkhurst, UK) was employed to regulate the air injected into the foam generator. The foam quality was regulated by changing the flow rate of gas ($q_g$) and surfactant solution ($q_l$) as it can be calculated from $q_g/(q_g+q_l)$. All foam displacement measurements were carried out at foam quality and gas flow rate of 90% with gas flow rate of 10 mL/min, respectively. The foam was injected inside the Hele-Shaw cell until the pressure profile reached the steady state condition. Then, after the flow rate stopped, the evolution of foam bubbles was monitored over time. Each experiment was repeated five times and, the results presented are the average of these experiments. Error bars represent standard

deviations. Both foamability and foam stability were investigated using a high-resolution camera. The automated monochromic camera (Dalsa Genie TS-2500), with a resolution of 2560×2048 pixels, was mounted above, to record the flow displacement inside the Hele-Shaw cell.

*2.4.2 Glass Bead Experiments.* A cell with a similar design to the Hele-Shaw cell described above was used for glass-bead experiments (Figure S1 in the Supporting information). The two plates were fixed permanently with a gap of 2 mm using several screws fitted around the cell. The fine silica glass-beads with a diameter size of 0.3-0.5 mm were packed inside the cell. To calculate the porosity, the total volume of the empty Hele-Shaw cell ($V_{total}$) was measured by the required volume of water to fill up the empty Hele-Shaw cell. Then, the needed volume of water to fill the Hele-Shaw with the glass bead inside ($V_{pore}$) was measured. Accordingly, the porosity can be calculated from $V_{pore}/V_{total}$. The porosity of the system was approximately 35%. Foam flow experiments were performed in the presence and absence of oil using pre-generated foam at 10 mL.min$^{-1}$ of gas flow rate. The pressure drop profile was recorded versus time in each experiment.

*2.4.3. Image Processing.* Image processing was performed in a similar fashion to that described previously.[17] The images captured using the monochromic camera for each experiment were segmented and analyzed by the utilization of ImageJ software. Hence, the image modification implemented in the sequence as follows: a) image segmentation was

performed by enabling the 'Bandpass Filter' tool on each image, b) the 'brightness/contrast' was adjusted to illuminate the bubbles whilst eliminating any evidence of background noise, c) the 'Threshold' tool was used to transform the image into a black and white format for better visual observation, and d) an analysis tool in ImageJ called 'Analyze Particles' was applied to determine the number of bubbles present.

## 3. RESULTS AND DISCUSSION

**3.1. Interfacial Properties of Surfactants in Water and at W/O Interface.** To investigate the effect of surfactant properties on foam stability, interfacial tensions of aqueous surfactant solutions in air or in oil were measured by pendant drop method. Interfacial properties obtained from the measurements for two anionic surfactants (FG4 and LSES, with the structure shown in Figure 1a and b, respectively) were compared with two commercially available anionic (SDS, Figure 1c) and cationic (CTAB, Figure 1d) surfactants. The CMC, surface tension and IFT of the respective surfactant solutions are presented in Table 1.[26,27]

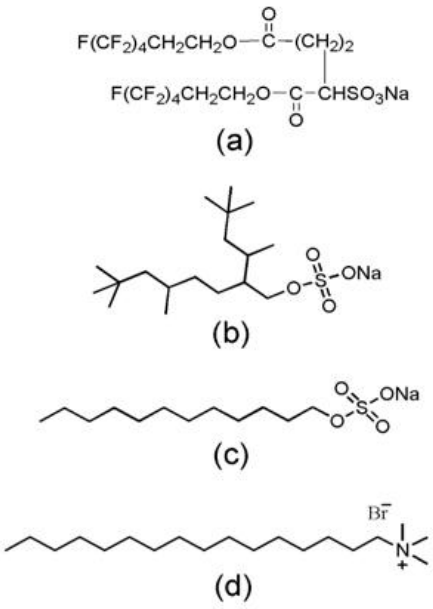


**Figure 1.** Structure of the surfactants used herein: (a) FG4, (b) $iC_{18}S$(FO-180) (LSES), (c) SDS, and (d) CTAB.

**Table 1.** Krafft point, CMC, and surface tension (σ) of surfactants used in the present study in pure water at 25 °C. Surface tension and IFT values were measured at CMC.

| Surfactant | Charge | Krafft point (°C)[a] | CMC ($10^{-3}$ mol $L^{-1}$) | Surface tension (mN $m^{-1}$) | Static IFT values (mN $m^{-1}$) | |
|---|---|---|---|---|---|---|
| | | | | | Oil | Asphaltenic oil |
| FG4 | Anionic | < 0 | 2.6 (±0.1) | 18.0 (±0.5) | 9.5 (±1.5) | 19 (±1.5) |
| LSES | Anionic | < 25 | 2.7 (±0.1) | 26.5 (±1.5) | 0.5 (±0.2) | 0.4 (±0.2) |
| SDS | Anionic | 15 | 8.2 (±0.1) | 32.3 (±1.4) | 6.2 (±2.0) | 4.5 (±2.0) |
| CTAB | Cationic | 24.5 | 0.9 (±0.2) | 35.2 (±1.5) | 11.1 (±1.0) | 10.2 (±1.0) |

[a] Krafft point is defined as the minimum temperature required for micelle formation in a solution, and these were obtained from the literature.[26,27] The experimental errors (standard deviations) on the measurements have an average of five values.

FG4 exhibits a very low surface tension at its critical micelle concentration (CMC) compared to the other surfactants, which is most likely due to the combination of (a) lower cohesive energy density caused by weak van der Waals interactions between fluorocarbon chains (*cf.,* Fig. 1a), (b) smaller polarizability of perfluoroalkyl as compared to hydrocarbon substituents, (c) higher hydrophobicity, due to a larger molecular volume of perfluoroalkyl than hydrocarbon moieties, and (d) higher packing density due to the greater cross-section of fluorocarbon chains.[28,29] We note that long-chain fluorocarbon surfactants are well known to provide lower surface tensions than those of hydrocarbon surfactants,[28,30] but short FC-chain surfactant FG4 is also found to generate the low surface tension comparable to those whilst also reducing disadvantages originating from FCs being bio-accumulative and environment-burdensome.

A relatively low surface tension of 26.5 mN/m (for a single chain surfactant) is observed for LSES at its CMC = 2.7 mM. The lower surface tension of LSES solutions is in agreement with the results obtained in previous studies,[31,24] and can be explained by (a) the higher $CH_3/CH_2$ ratio and (b) the increased packing efficiency of the branched hydrophobic tails against the electrostatic repulsion between the anionic sulfate head-groups in the adsorption layer.[13,24,32] All these results support the concept that the surface tension depends on the surfactant molecular structure and that the surface energy increases with the tail-composition in the sequence $CF_3 < CF_2 < CH_3 < CH_2$.[30,33]

**3.2. Rheological properties of various aqueous surfactant systems.** One of the main factors for stabilized foam is its rheological properties in the aqueous surfactant solution. exhibits variation of the surfactant solution viscosity (η, mPa.s) and the shear stress (τ, Pa) as a function of the shear rate (γ, $s^{-1}$) at 25 ℃. The viscosity (η) of each surfactant solution (at CMC) decreases by increasing the shear rate (Figure 2a). At lower shear rates (0-35 $s^{-1}$), Phase I, the magnitude of viscosity follows: FG4 > LSES > SDS > CTAB. This trend can be attributed to varying headgroup, and surfactant monomers aligning with the flow.

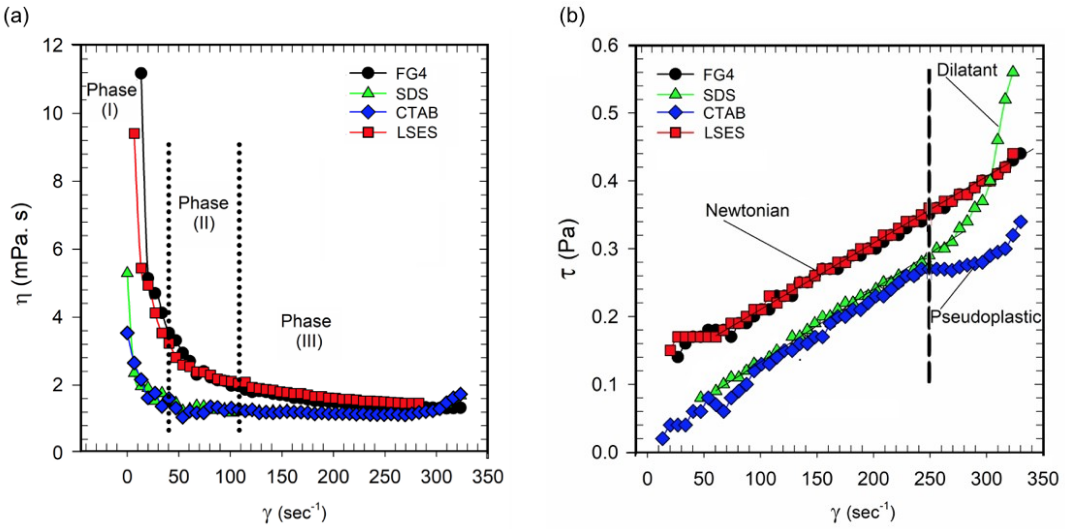


**Figure 2.** Time-dependence (a) viscosity (η) versus shear rate ($sec^{-1}$) and (b) shear stress (τ) versus shear rate ($sec^{-1}$) curves for surfactant solutions over $sec^{-1}$. The errors in the viscosity and shear stress are ±0.5 mPa.s and ±0.02 Pa, respectively.

To determine whether the surfactant solution has a Newtonian and non-Newtonian behavior, we have carefully investigated Region II and III (35-350 $s^{-1}$), shows that while the apparent viscosity decreases during Region II and III, the shear stress is increasing the shear rate (Figure 2b). Typically, surfactant solutions behave as non-Newtonian fluid, although pseudo-plastic and dilatant behavior responses must be taken into account when considering CTAB and SDS after

230 and 290 $sec^{-1}$, respectively. In the final region (Region III), extreme shear rate shows viscosity of FG4 and SDS tends to be constant (100-350 $s^{-1}$), while a pseudo-plastic and dilatant (shear-thickening) behavior was observed for CTAB and SDS, respectively.

**3.3. Foam flow and coarsening in Hele-Shaw cell.** The foam stability was initially evaluated by flooding an empty Hele-Shaw cell with pre-generated foam. After reaching the steady-state condition, the injection was stopped, and the evolution of stagnant foam bubbles was observed over time as depicted in Figure 3.

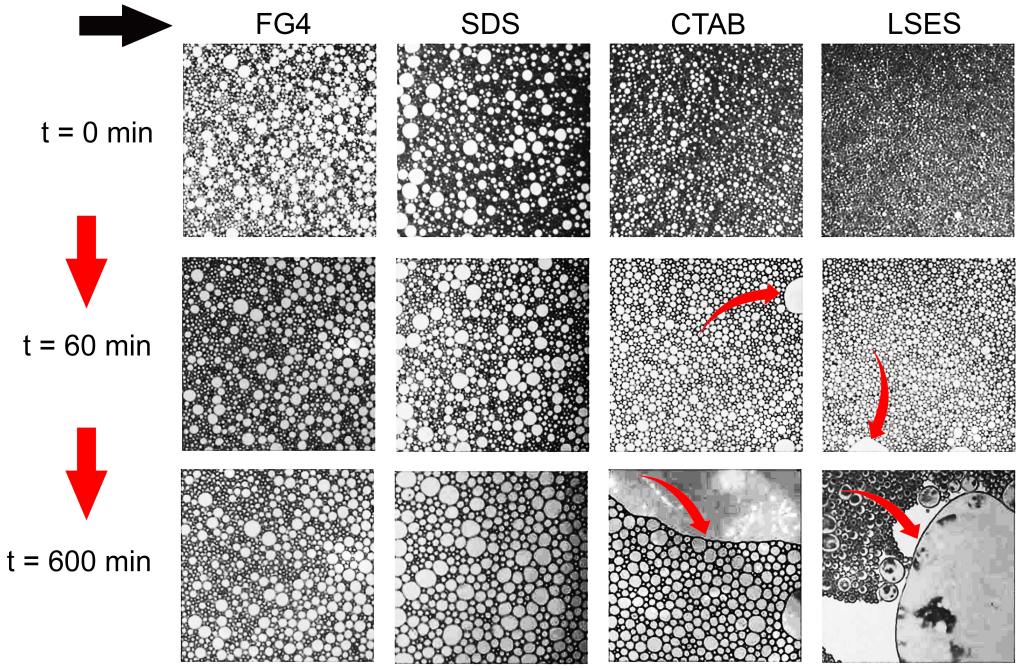


**Figure 3.** Illustrative pictures of foam stability for the FG4, SDS, CTAB, and LSES in the empty Hele-Shaw cell at 0 min, 60 min and 600 min at 25 °C.

Quantitatively, the time-dependent plots of the number of foam bubbles and the pressure drop across the device are shown in Figure 4. For LSES more than thirty thousand of very small bubbles formed with LSES at t = 0. The bubble number was almost double that for CTAB, triple that for FG4, and quadruple that for SDS, suggesting the high foamability of LSES. It is very

interesting to note that LSES can show higher foamability than FG4 at almost same concentrations (CMC = 2.6 and 2.7 mM) although $\sigma_{CMC}$ of LSES was higher by 8.5 mN/m than that of FG4. At time < 100 min, the number and size of bubbles formed by LSES remained as the largest and smallest respectively out of the surfactants tested. After 100 min, bubbles prepared by FG4 became the smallest in average size and the largest in number. To assess the foam stability at bubble-scale, the ratio of $N_i/N_t$ versus time were shown in Figure S3 in Supporting Information, where $N_i$ is the initial number of foam bubbles at time zero and $N_t$ is the number of bubbles over time. The slope of this plot represents the bubble-coarsening rate of the studied foams.

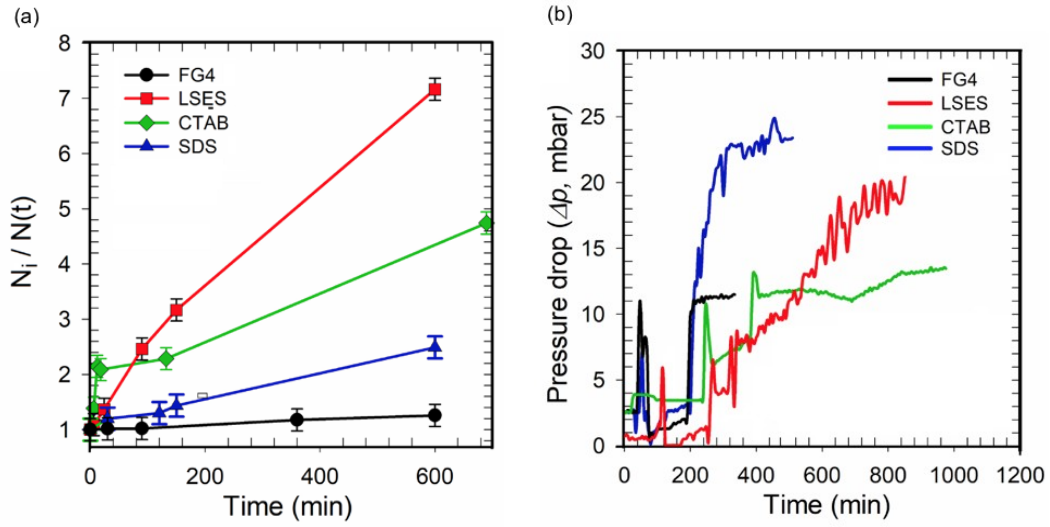


**Figure 4.** Plots of (a) the total number of bubbles at time *t* ($N_t$) versus time and (b) the pressure drop versus time during foam flow in an initially empty Hele-Shaw cell.

Figure 4b displayed higher foam coarsening rates for LSES and CTAB than for SDS at t = 0-100 min. This can be attributed to the larger numbers of smaller bubbles for LSES and CTAB, which cause larger water/air interface (lamellae) areas generating a higher total surface free energy. According to Table 1, the CMC values of LSES and CTAB in terms of molar

concentration are just $^1/_3$ and $^1/_9$ of the values for SDS, respectively. This then implies the movement of the surfactant molecules to the interfaces and the need to spread them over the very large interfacial areas. As a consequence, there is a reduction of the surfactant molecule concentration on the interfaces, which leads to a rise in surface tension and a decrease in electrostatic repulsion between bubbles, causing high foam coarsening rate. When the slopes in Figure 4a are compared at low bubble numbers $N_t$ <5000, those for the hydrocarbon surfactants (LSES, SDS and CTAB) are similar, suggesting the stability LSES was not so bad when bubble numbers were fewer and hence interfacial area was less (i.e., less depletion).[21]

Interestingly, FG4 despite its comparatively low CMC value shows a low coarsening rate compared to the other surfactants. This can be due to its high surface elasticity and low surface energy generated by a monolayer of FG4 having rigid fluorocarbon tails leading to strong hydrophobicity and gas-philicity and a film-oriented architecture (double tail + single headgroup) producing a larger packing parameter than a single tail surfactant. Indeed, as Figure 1 shows this surfactant has two branches of similar size. Hence, we can expect it can cover more surface area of the foam bubbles and then stabilize lamellae. Low fluctuations in pressure drop profile for FG4 surfactant is another indication of its high stabilizing ability.

**3.4. Oil Displacement with and without Asphaltene Aggregates.** We studied foam flow behavior in the presence of oil, as shown in Figure 5. These results show the detrimental effect of oil on foam stability for all surfactant solutions, except the FG4. The bubble coalescence is very intensive for CTAB, SDS, and LSES even in the first seconds after the foam contact with oil. The oil acts as an active antifoam agent with respect to the foams stabilized by hydrocarbon surfactants (especially SDS and CTAB), causing intensive bubble coalescence.[30] In

contrast, foams generated in FG4 solution were very stable. At $t$ = 90 sec (right-hand column in Figure 5) the FG4 foam displaced the oil from the Hele-Shaw cell without any bubble coalescence or coarsening, which is undoubtedly due to the specific molecular structure of fluorocarbon surfactant. The observed remarkable stability of the FG4-stabilized foam, upon contact with the oil, can be due to its high surface viscosity and immiscibility between the fluoroalkyl moieties within the FG4 surfactant and the hydrocarbon.[34]

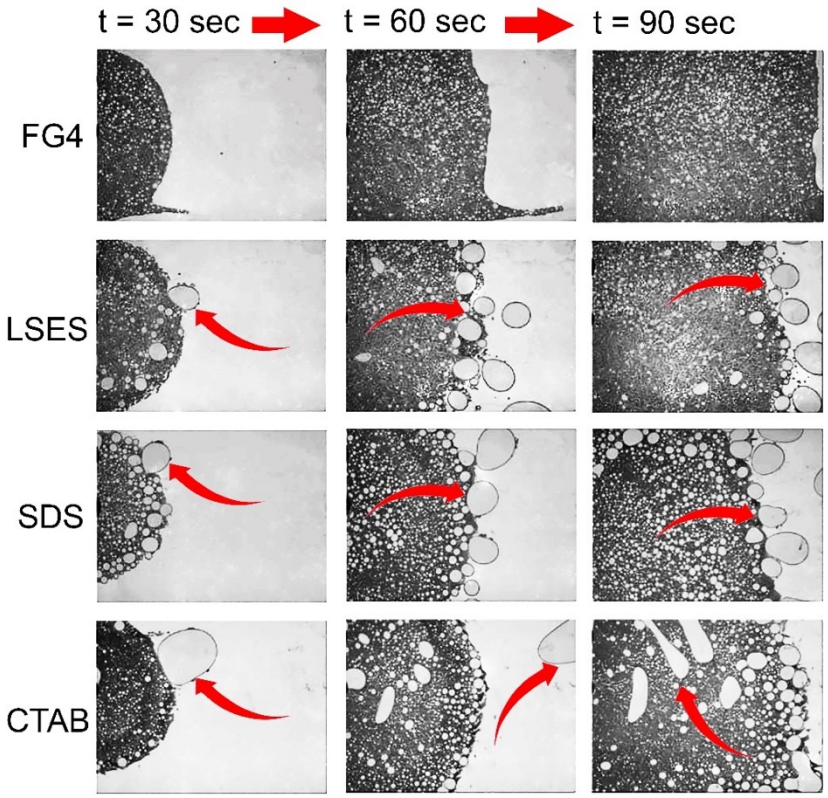


**Figure 5.** Oil displacement with different foam systems as presented in the legend. The arrows show large amount of bubble coalescence in the presence of oil over time.

Similar series of experiments were carried out in the presence of asphaltene, as presented in Figure 6. The foams generated from FG4 solution in asphaltene-oil showed very high foam stability at $t$ = 30 sec with a bubble size similar to that of FG4 in oil, while the foams from LSES,

SDS, and CTAB were particularly unstable. The bubble coalescence was more intensive in the CTAB foam compared to the LSES and SDS. At $t$ = 60 and 90 sec (middle and right-hand columns in Figure 6, respectively), significant foam film rupture and bubble coalescence was observed in the foams stabilized by CTAB, SDS or LSES. A comparison of Figure 5 with Figure 6 suggests that asphaltene in oil has a powerful antifoam effect for the foams stabilized by hydrocarbon surfactants. Most probably, the adsorption of surfactant molecules to the asphaltene aggregate deprive the lamellae from having enough surfactant to be stabilized. In contrast, asphaltene had no significant effect on the foam stability for FG4 which may be due to the immiscibility between these two due to its specific molecular structure and its higher viscosity.

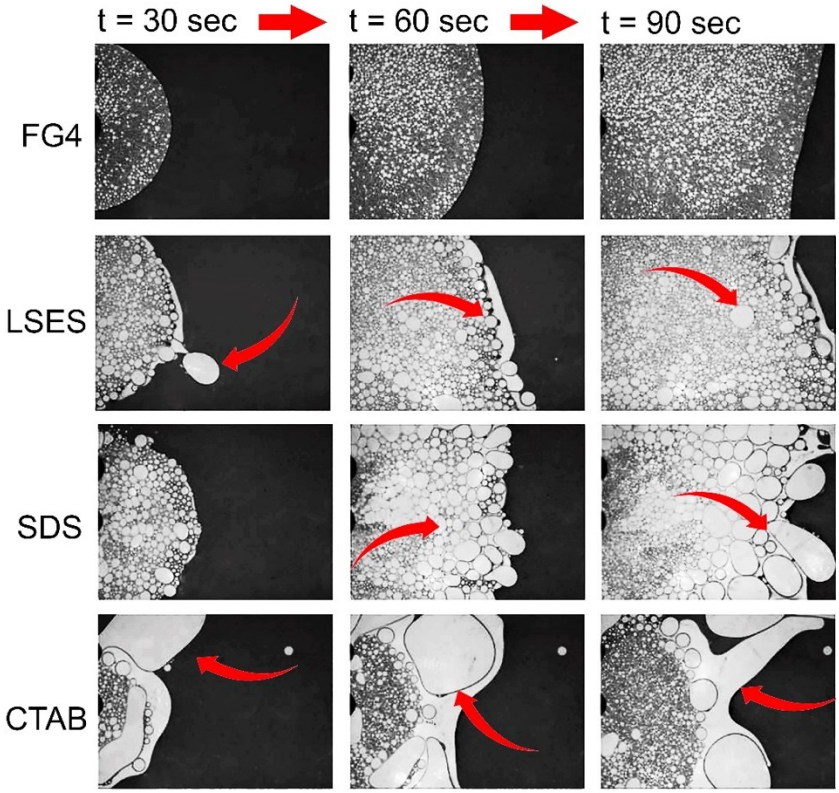

**Figure 6.** Illustrative pictures of foam stability and foam displacement in the Hele-Shaw cell for FG4, SDS, CTAB, and LSES in the case of asphaltene-oil at three successive times of 30, 60 and 90 sec. The arrows indicate the foam coalescence for each foam surfactant solution.-

**3.5. Foam flow in porous media.** To highlight the role of capillary suction on foam stability, a series of foam flow experiments inside more complex confined geometries were performed using a glass bead pack. Foam saturation and pressure drop measurements with the corresponding displaced fluid (water, oil, and asphaltene-oil) were plotted in Figure 7. Foam saturation is the proportion of the glass bead pack that is filled with foam.

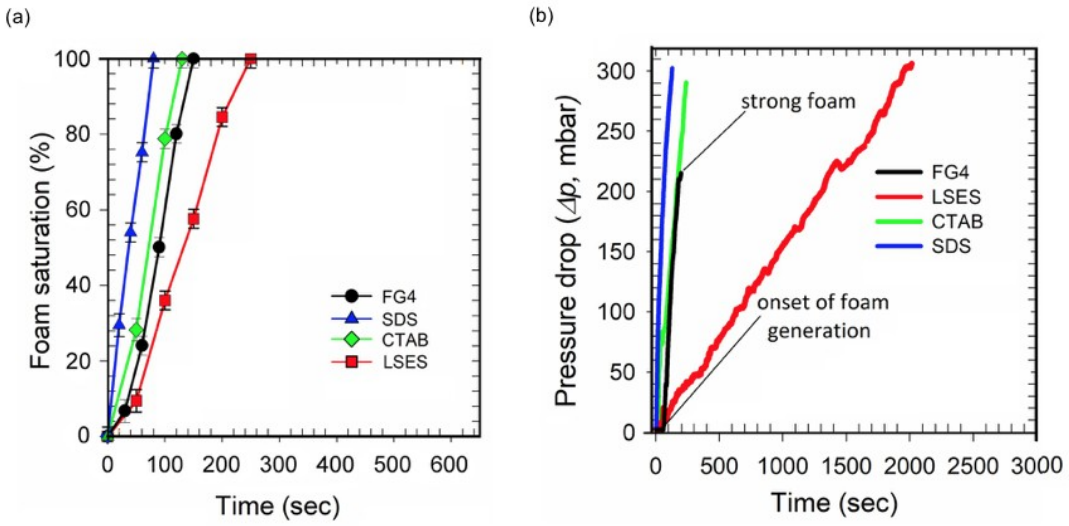


**Figure 7.** Plots of (a) foam saturation and (b) pressure drop during water displacement by foam in the glass bead pack for different surfactants as presented in the legends. For interpretation of different color lines, the reader is referred to the online version of this article.

For displacement of water, higher foam saturation was observed for the SDS, CTAB, and FG4 compared to LSES surfactant. This was attributed to the comparatively rapid breakage of bubbles made with LSES (as Figure 4 shows). The pressure-drop curves in (b) show that SDS,

CTAB, and FG4 create a strong foam bank zone in the water quite similar to the case of empty Hele-Shaw cell. Decreased foam saturation was observed when foam displaced oil compared to foam displacing water, which weakened the foam films, leading to bubble coalescence (Figure 8).

The presence of oil, significantly decreases the foam saturation and effectively increases gas channeling in the direction of flow, compared to foam saturation in the presence of water. The foam saturation in the presence of oil (Figure 8) is ranked as follows: FG4 > LSES > SDS > CTAB. Again, very high foam stability as a function of time was obtained for FG4, which agrees with the results shown in Figure 3; however, LSES foam appeared to be more stable compared to the CTAB and SDS. This can be due to a lower miscibility of the hyper-methyl-branched hydrocarbon tail of LSES with the oil than the straight hydrocarbon tails of SDS and CTAB (Fig. 1).[35,36] Figure 9 shows foam saturation and pressure drop during asphaltenic oil displacement by foam. Comparing Figure 9 with Figure 8 reveals the detrimental effect of asphaltene on foam stability.

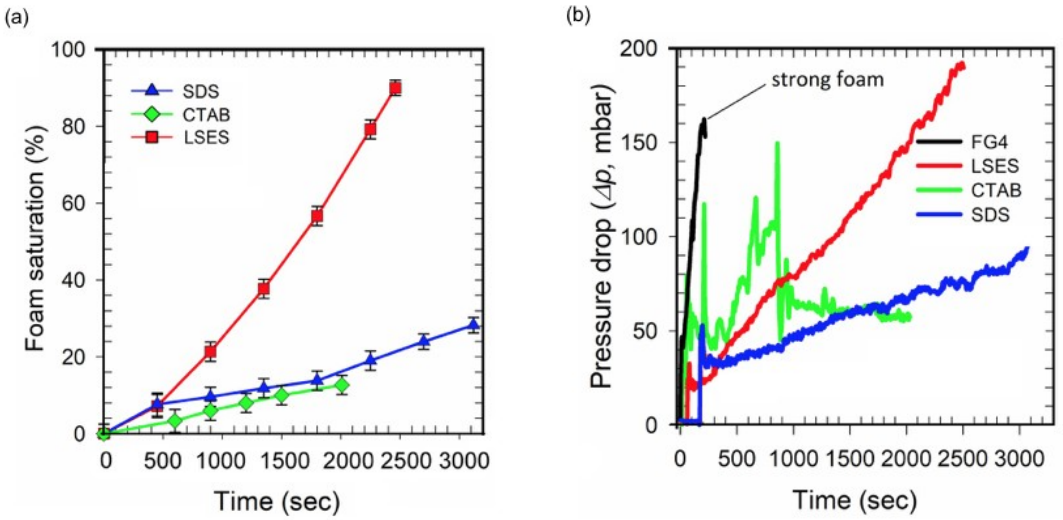

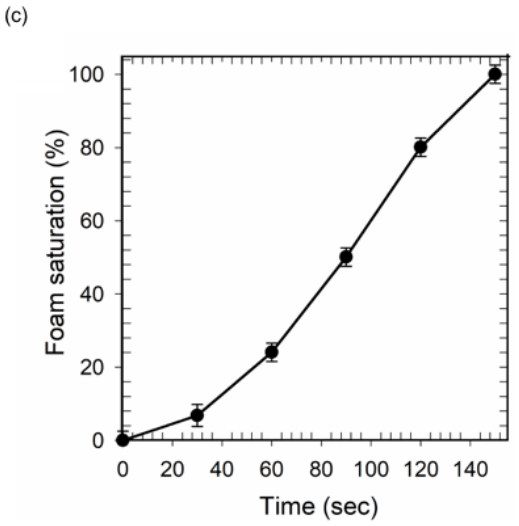


**Figure 8.** Plots of (a) foam saturation and (b) pressure drop in the case of SDS, CTAB, and LSES, at CMC during oil displacement in the glass bead pack. (c) Foam saturation of FG4 displacing oil in the glass bead pack (plotted separately on a different scale). For interpretation of different color lines, the reader is referred to the online version of this article.

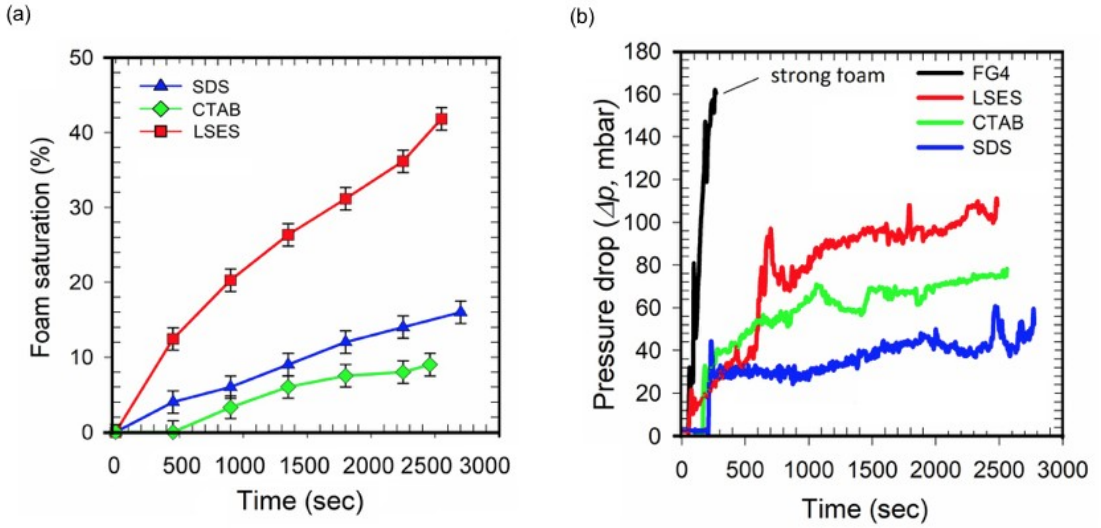

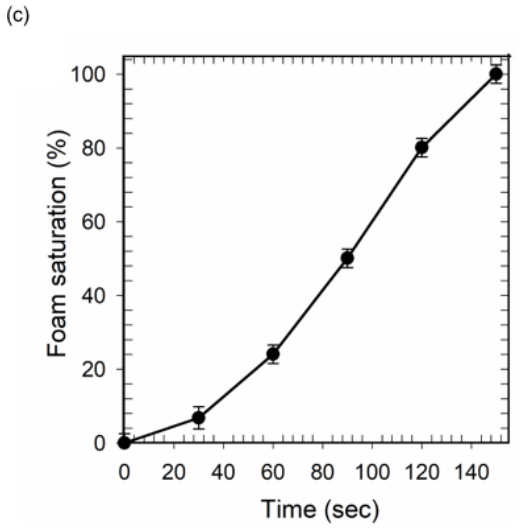


**Figure 9.** (a) Foam saturation and (b) displacement pressures in asphaltene-oil for SDS, CTAB, and LSES at CMC in the glass bead pack. (c) Foam saturation of FG4 displacing asphaltene-oil in the glass bead pack (plotted separately). For interpretation of different color lines, the reader is referred to the online version of this article.

Apart from FG4, foam saturation considerably reduced across all solutions in asphaltene-oil, as shown in Figure 8. FG4 saturates the entire system more rapidly (160 sec) than other foam systems. Highly stable foam is expected to control gas mobility and decrease gas channeling during foam displacement in the glass bead pack. The ranking of the order in which surfactants successfully displaced asphaltenic oil as is as follows: FG4 > LSES > SDS >CTAB. It can be expected the adsorption of surfactant from lamellae to asphaltene aggregate destabilize the foam; however, the fluorocarbon tails in FG4 and hyper-methyl-branched tail in LSES is an obstacle to this phenomenon that provides higher stability behavior for these novel surfactants.

In this study, we focused on surfactants at their CMC concentration; however, surfactant concentration can have a very important role on foam stability and generation that could be the topic of future study.[21]

## 4. CONCLUSIONS

Although previous studies have discussed foam stability extensively,[37,38] this study significantly advances this research area since it not only used newly developed surfactants with specific properties, but also critically explored the effect of asphaltene aggregates on foam stability. In addition to the real-world importance of studying asphaltene containing systems, the effects of its presence should not be discounted. The strong hydrophobicity and good gas-philicity, and weak interaction with the oil of hydrophobic tails, and the film-oriented architecture, which is likely to increase the packing parameter for FG4 and LSES surfactant make them more stable in the presence of oil and asphaltenic oil compared to the more traditional SDS and CTAB surfactants. These results pave the road for designing new surfactants with a high ability to stabilize foam in extreme systems.

### ASSOCIATED CONTENT

### Supporting Information

The Supporting Information is available free of charge on the ACS Publications website at DOI: XXXXXX.

Hele-Shaw cell or in glass-bead porous media as well as dynamic IFT data (PDF).

## AUTHOR INFORMATION

### Corresponding Author

*E-mail: nima.shokri@tuhh.de (N. Shokri)

*E-mail: s.alexander@swansea.ac.uk (S. Alexander)

*E-mail: a.r.barron@swansea.ac.uk (A.R. Barron).

### Author Contributions

The manuscript was written through contributions of all authors. All authors have given approval to the final version of the manuscript.

### Declaration of Competing Interest

The authors declare that they have no known competing financial interests or personal relationships that could have appeared to influence the work reported in this paper.

## ACKNOWLEDGMENT

The Welsh Government Sêr Cymru Programme provided financial support through Sêr Cymru II Welsh Fellowship part-funded by the European Regional Development Fund (ERDF), the Sêr Cymru Chair for Low Carbon Energy and Environment, the Reducing Industrial Carbon Emissions (RICE) operations funded by the Welsh European Funding Office (WEFO) through the Welsh Government, KAKENHI (Fund for the Promotion of Joint International Research (Fostering Joint International Research (A)) No. 15KK0221, Grant-in-Aid for Challenging Research (Exploratory), No.17K19002, and Grant-in-Aid for Scientific Research (B), No.

19H02504) founded by JSPS. We acknowledge the University of Manchester for providing the PhD studentship for Mohammad Javad Shojaei. The experiments with the Hele-Shaw cell were conducted at The University of Manchester.

## ABBREVIATIONS

CTAB = cetyl trimethyl ammonium bromide

CMC = critical micelle concentration

EOR = enhanced oil recovery

FG4 = sodium 1,5-*bis*[(*1H,1H,2H,2H*-perfluorohexyl)oxy]-1,5-dioxopentane-2-sulfonate

IFT = interfacial tension

$q_g$ = flow rate of gas

$q_l$ = surfactant solution

γ = shear rate

η = viscosity

σ = surface tensions

τ = shear stress

LSES = low surface energy surfactant

$N_t$ = number of bubbles at time

$N_i$ = initial number of foam bubbles

SDS = sodium dodecyl sulfate

$V_{total}$ = total volume of the empty Hele-Shaw cell

$V_{pore}$ = volume of water to fill the Hele-Shaw with the glass bead inside

## REFERENCES

(1) Petkova, B.; Tcholakova, S.; Chenkova, M.; Golemanov, K.; Denkov, N.; Thorley, D.; Stoyanov, S. Foamability of aqueous solutions: Role of surfactant type and concentration, *Adv. Colloid Interface Sci.* **2020**, *276*, 102084. https://doi.org/10.1016/j.cis.2019.102084.

(2) Shojaei, M. J.; Osei-Bonsu, K.; Richman, S.; Grassia, P.; Shokri, N. Foam stability influenced by displaced fluids and by pore size of porous media, *Ind. Eng. Chem. Res.* **2018**, *58*, 1068-1074. https://doi.org/10.1021/acs.iecr.8b05265.

(3) Wang, S.; Mulligan, C. N. An evaluation of surfactant foam technology in remediation of contaminated soil. *Chemosphere* **2004**, *57*, 1079-1089. https://doi.org/10.1016/j.chemosphere.2004.08.019.

(4) Beneventi, D.; Carre, B.; Gandini, A. Role of surfactant structure on surface and foaming properties. *Colloids Surf. A Physicochem. Eng. Asp.* **2001**, *189*, 65-73. https://doi.org/10.1016/S0927-7757(01)00602-1.

(5) Tan, S. N.; Fornasiero, D.; Sedev, R.; Ralston, J. The role of surfactant structure on foam behaviour. *Colloids Surf. A Physicochem. Eng. Asp.* **2005**, *263*, 233-238. https://doi.org/10.1016/j.colsurfa.2004.12.060.

(6) Hong, C. R.; Park, S. J.; Choi, S. J. Influence of the hydrophilic head size and hydrophobic tail length of surfactants on the ability of micelles to stabilize citral. *J. Sci. Food Agric.* **2016**, *96*, 3227-3232. https://doi.org/10.1002/jsfa.7505.

(7) Kanduč, M.; Schneck, E.; Stubenrauch, C. Intersurfactant H-bonds between head groups of n-dodecyl-β-d-maltoside at the air-water interface. *J. Colloid Interf. Sci.* **2021**, *586*, 588-595. https://doi.org/10.1016/j.jcis.2020.10.125.

(8) Hait, S. K.; Moulik, S. P. Determination of critical micelle concentration (CMC) of nonionic surfactants by donor-acceptor interaction with Iodine and correlation of CMC with

hydrophile-lipophile balance and other parameters of the surfactants. *J. Surfactants Deterg.* **2001**, *4*, 303-309. https://doi.org/10.1007/s11743-001-0184-2.

(9) Lin, S.-Y.; Lin, Y.-Y.; Chen, E.-M.; Hsu, C. T.; Kwan, C. C. A study of the equilibrium surface tension and the critical micelle concentration of mixed surfactant solutions. *Langmuir* **1999**, *15*(13), 4370-4376. https://doi.org/10.1021/la981149f.

(10) Kiani, S.; Alexander, S.; Barron, A. R. *Emerging Platforms in Fluid Flow Transport: Surfactants, Polymers, and Nanoparticles*, Lulu Press, Inc., Morrisville, NC (2021). ISBN:978-1838416706.

(11) Lioumbas, J. S.; Georgiou, E.; Kostoglou, M.; Karapantsios, T. D. Foam free drainage and bubbles size for surfactant concentrations below the CMC. *Colloids Surf. A Physicochem. Eng. Asp.* **2015**, *487*, 92-103. https://doi.org/10.1016/j.colsurfa.2015.09.050.

(12) Vikingstad, A. K.; Skauge, A.; Høiland, H.; Aarra, M. Foam–oil interactions analyzed by static foam tests. *Colloids Surf. A Physicochem. Eng. Asp.* **2005**, *260*, 189-198. https://doi.org/10.1016/j.colsurfa.2005.02.034.

(13) Yekeen, N.; Manan, M. A.; Idris, A. K.; Samin, A. M. Influence of surfactant and electrolyte concentrations on surfactant Adsorption and foaming characteristics. *J. Pet. Sci. Eng.* **2017**, *149*, 612-622. https://doi.org/10.1016/j.petrol.2016.11.018.

(14) Wang, J.; Nguyen, A. V.; Farrokhpay, S. A critical review of the growth, drainage and collapse of foams. *Adv. Colloid Interface Sci.* **2016**, 228, 55-70. https://doi.org/10.1016/j.cis.2015.11.009.

(15) Shojaei, M. J.; Osei-Bonsu, K.; Grassia, P.; Shokri, N. Foam flow investigation in 3D-printed porous media: fingering and gravitational effects. *Ind. Eng. Chem. Res.* **2018**, *57*, 7275-7281. https://doi.org/10.1021/acs.iecr.8b00136.

(16) Manev, E.; Sazdanova, S.; Wasan, D. Emulsion and foam stability-the effect of film size on film drainage. *J. Colloid Interface Sci.* **1984**, 97, 591-594. https://doi.org/10.1016/0021-9797(84)90334-5.

(17) Shojaei, M. J.; Rodríguez de Castro, A.; Méheust, Y.; Shokri, N. Dynamics of foam flow in a rock fracture: Effects of aperture variation on apparent shear viscosity and bubble morphology. *J. Colloid Interface Sci.* **2019**, 552, 464-475. https://doi.org/10.1016/j.jcis.2019.05.068.

(18) Salonen, A.; Lhermerout, R.; Rio, E.; Langevin, D.; Saint-Jalmes, A. Dual gas and oil dispersions in water: production and stability of foamulsion. *Soft Matter* **2012**, *8*, 699-706. https://doi.org/10.1039/C1SM06537H.

(19) Simjoo, M.; Rezaei, T.; Andrianov, A.; Zitha, P. L. J. Foam stability in the presence of oil: effect of surfactant concentration and oil type. *Colloids Surf. A Physicochem. Eng. Asp.* **2013**, *438*, 148-158. https://doi.org/10.1016/j.colsurfa.2013.05.062.

(20) Farajzadeh, R.; Andrianov, A.; Krastev, R.; Hirasaki, G. J.; Rossen, W. R. Foam–oil interaction in porous media: implications for foam assisted enhanced oil recovery. *Adv. Colloid Interface Sci.* **2012**, *183*, 1-13. https://doi.org/10.1016/j.cis.2012.07.002.

(21) Boos, J.; Drenckhan, W.; Stubenrauch, C. On how surfactant depletion during foam generation influences foam properties. *Langmuir* **2012**, *28*, 9303-9310. https://doi.org/10.1021/la301140z.

(22) Jones, S. A.; Laskaris, G.; Vincent-Bonnieu, S.; Farajzadeh, R.; Rossen, W. R. Effect of surfactant concentration on foam: from coreflood experiments to implicit-texture foam-model parameters. *J. Ind. Eng. Chem.* **2016**, *37*, 268-276. https://doi.org/10.1016/j.jiec.2016.03.041.

(23) Kiani, S.; Rogers, S. E.; Sagisaka, M.; Alexander, S.; Barron, A. R. A new class of low surface energy anionic surfactant for enhanced oil recovery (EOR), *Energy Fuels* **2019**, *33*, 3162-3175. https://doi.org/10.1021/jp0270957.

(24) Sagisaka, M.; Iwama, S.; Ono, S.; Yoshizawa, A.; Mohamed, A.; Cummings, S.; Yan, C.; James, C.; Rogers, S. E.; Heenan, R. K. Nanostructures in water-in-$CO_2$ microemulsions stabilized by double-chain fluorocarbon solubilizers, *Langmuir* **2013**, *29*, 7618-7628. https://doi.org/10.1021/la400376g.

(25) Alexander, S.; Smith, G. N.; James, C.; Rogers, S. E.; Guittard, F.; Sagisaka, M.; Eastoe, J. Low-surface energy surfactants with branched hydrocarbon architectures, *Langmuir* **2014**, *30*, 3413-3421. https://doi.org/10.1021/la500332s.

(26) Vautier-Giongo, C.; Bales, B. L. Estimate of the ionization degree of ionic micelles based on Krafft temperature measurements, *J. Phys. Chem. B.* **2003**, 107, 5398-5403. https://doi.org/10.1021/jp0270957.

(27) Manojlovic, J. Ž. The Krafft temperature of surfactant solutions, *Therm. Sci.* **2012**, *16*, S631-S640. https://doi.org/10.2298/TSCI120427197M.

(28) Nowicki, J.; Sokołowski, A.; Reksa, D. Synthesis and surface-active properties of novel carbohydrate-based cationic surfactants, *J. Surf. Det.* **2011**, *14*, 179-184. https://doi.org/10.1007/s11743-010-1225-4.

(29) Krafft, M. P.; Riess, J. G. Chemistry, physical chemistry, and uses of molecular fluorocarbon-hydrocarbon diblocks, triblocks, and related compounds-unique "apolar" components for self-assembled colloid and interface engineering, *Chem. Rev.* **2009**, *109*, 1714-1792. https://doi.org/10.1021/cr800260k.

(30) Kovalchuk, N. M.; Trybalaa, A.; Starova, V.; Matar, O.; Ivanova, N. Fluoro- vs hydrocarbon surfactants: Why do they differ in wetting performance? *Adv. Colloid Interface Sci.* **2014**, *210*, 65-71. https://doi.org/10.1016/j.cis.2014.04.003.

(31) Kiani, S.; Jones, D. R.; Alexander, S.; Barron, A. R. New insights into the interactions between asphaltene and a low surface energy anionic surfactant under low and high brine salinity. *J. Colloid Interface. Sci.* **2020**, *571*, 307-317. https://doi.org/10.1016/j.jcis.2020.03.018.

(32) Borges, L. G. A.; Savi, A.; Teixeira, C.; deOliveira, R. P.; de Camillis, M. L. F.; Wickert, R.; Brodt, S. F. M.; Tonietto, T. F.; Cremonese, R.; Silva, L. S.; Gehm, F.; Oliveira, E. S.; Barth, J. H. D.; Macari, J. G.; Barros, C. D.; Vieira, S. R. R. Mechanical ventilation weaning protocol improves medical adherence and results. *J. Crit. Care* **2017**, *41*, 296-302. https://doi.org/10.1016/j.jcrc.2017.07.014.

(33) Czajka, A.; Hazell, G.; Eastoe, J. Surfactants at the design limit, *Langmuir* **2015**, *31*, 8205-8217. https://doi.org/10.1021/acs.langmuir.5b00336.

(34) Stubenrauch, C.; Hamann, M.; Preisig, N.; Chauhan, V.; Bordes, R. On how hydrogen bonds affect foam stability. *Adv. Colloid Interface Sci.* **2017**, *247*, 435-443. https://doi.org/10.1016/j.cis.2017.02.002.

(35) Wu, X.; Zhao, J.; Li, E.; Zou, W. Interfacial dilational viscoelasticity and foam stability in quaternary ammonium gemini surfactant systems: influence of intermolecular hydrogen bonding. *Colloid Polym. Sci.* **2011**, *289*, 1025-1034. https://doi.org/10.1007/s00396-011-2425-9.

(36) Yekeen, N.; Manan, M.; Idris, A. K.; Padamanabhan, E.; Junin, R.; Samin, A. M.; Oguamah, I. A comprehensive review of experimental studies of nanoparticles-stabilized foam for enhanced oil recovery, *J. Petro. Sci. Eng.* **2018**, *164*, 43-47. https://doi.org/10.1016/j.petrol.2018.01.035.

(37) Xiao, S.; Zeng, Y.; Vavra, E.; He, P.; Puerto, M.; Hirasaki, J. G.; Biswal, S. L. Destabilization, propagation, and generation of surfactant-stabilized foam during crude oil displacement in heterogeneous model porous media, *Langmuir* **2018**, *34*, 739–749. https://doi.org/10.1021/acs.langmuir.7b02766.

(38) La Mesa, C.; Ranieri, G.; Terenzi, M. Studies on Krafft point solubility in surfactant solutions, *Thermochimica Acta* **1988**, *137*, 143-150. https://doi.org/10.1016/0040-6031(88)87476-8.

## Graphical Abstract